

# BRU59-21, a Second-Generation $^{99m}\text{Tc}$ -Labeled 2-Nitroimidazole for Imaging Hypoxia in Tumors

Tricia Melo, Jill Duncan, James R. Ballinger, and A. Michael Rauth

Departments of Medical Biophysics and Pharmacy, University of Toronto, Toronto; Division of Experimental Therapeutics, Ontario Cancer Institute, Toronto; and Division of Nuclear Medicine, University Medical Imaging Center, Toronto, Canada

Hypoxia in tumors is believed to be an important cause of local failure of radiotherapy in certain types of cancer. BRU59-21 (BMS194796) is a second-generation  $^{99m}\text{Tc}$ -labeled 2-nitroimidazole that has been shown to offer improved characteristics for imaging myocardial ischemia. It has now been evaluated in models of tumor hypoxia. **Methods:** Accumulation of BRU59-21 was compared with that of BMS181321 in Chinese hamster ovary cells incubated under aerobic or hypoxic conditions. The effects of competition with unlabeled nitroimidazoles and oxygen were studied. Biodistribution studies were performed in mice bearing transplanted KHT-C tumors in the leg. **Results:** Within 5 min, BRU59-21 partitioned into aerobic cells in vitro at a level 10 times higher than external medium with no further increase over time. In hypoxic cells this initial partitioning was followed by selective accumulation to levels 5 times higher than in aerobic cells by 4 h. Low levels of oxygen (~40 ppm) inhibited the maximal accumulation rate by 50%. Unlabeled misonidazole, a 2-nitroimidazole, inhibited accumulation of radioactivity, whereas tinidazole, a 5-nitroimidazole, enhanced accumulation; similar effects had been reported with BMS181321. Biodistribution studies in mice showed rapid clearance of radioactivity from the blood, resulting in enhanced tumor-to-blood ratios compared with BMS181321. Increasing the hypoxic fraction in the tumor by injection of nitro-L-arginine resulted in increased retention of tracer in the tumor without affecting other tissues. **Conclusion:** These results suggest that BRU59-21 warrants further investigation as an agent for imaging tumor hypoxia in the clinic.

**Key Words:** nitroimidazole;  $^{99m}\text{Tc}$ ; hypoxia; tumors

**J Nucl Med 2000; 41:169–176**

The first  $^{99m}\text{Tc}$ -labeled 2-nitroimidazole to be widely studied for imaging hypoxia is BMS181321 (Oxo[[3,3,9,9-tetramethyl-1-(2-nitro-1H-imidazol-1-yl)-4,8-diazaundecane-2,10-dione dioximato](3-)-N,N',N'',N''']-technetium; Fig. 1A) (1,2). Localization of BMS181321 has been shown in hypoxic cells in vitro and in hypoxic regions of brain, heart, and tumors in animal models (3–11), and there has been a preliminary report of the clinical evaluation of BMS181321 in acute stroke (12). Although these studies offer proof of the concept that  $^{99m}\text{Tc}$  chelated to a nitroimidazole can be

targeted to regions of hypoxia, the BMS181321 molecule has several limitations. It undergoes chemical decomposition in saline solutions and in cell-free growth medium, with a half-life of 16–20 h. Furthermore, its lipophilic nature (octanol–water partition coefficient, ~40), which allows it to cross the intact blood–brain barrier to image cerebral hypoxia, may make it suboptimal for imaging hypoxia in the heart or in tumors because of slow clearance from the blood and background tissues and extensive elimination through the liver and intestinal tract. In a previously reported evaluation of BMS181321 in mice bearing implanted murine tumors, the maximum values obtained were 4.2 for tumor-to-muscle ratios and 0.3 for tumor-to-blood ratios (8).

BRU59-21 (Oxo[[3,3,9,9-tetramethyl-5-oxa-6-(2-nitro-1H-imidazol-1-yl)-4,8-diazaundecane-2,10-dione dioximato](3-)-N,N',N'',N''']-technetium), previously known as BMS194796, (Fig. 1B) is a second-generation hypoxia agent with a chemical structure that differs from BMS181321 in that an oxygen atom has been substituted for a methylene group in the propylene bridge and the point of attachment of the 2-nitroimidazole has been moved from the 1 to the 6 position on the chelator (13,14). Preliminary reports suggest that these modifications have the effects of increasing chemical stability, reducing the octanol–water partition coefficient, and decreasing the level of radioactivity in the liver (13,14). BRU59-21 has been shown to possess superior properties for imaging myocardial hypoxia in an animal model (14). Here, we evaluate the behavior of BRU59-21 in models of tumor hypoxia in vitro and in mice and compare the results with previous work using BMS181321 in the same systems (8).

## MATERIALS AND METHODS

### Preparation of BRU59-21

BRU59-21 was prepared from research formulation kits (Bracco Research USA, Princeton, NJ). The ligand (BRU59, 400  $\mu\text{g}$ ) was dissolved in 800  $\mu\text{L}$  physiologic saline, and 100  $\mu\text{L}$  (185 MBq)  $^{99m}\text{Tc}$ -pertechnetate solution was added. The labeling reaction was initiated by adding 10  $\mu\text{g}$  stannous chloride and 500  $\mu\text{g}$  diethylenetriamine pentaacetic acid (DTPA) in 200  $\mu\text{L}$  saline (Bracco Techneplex kit reconstituted with 4 mL saline). After 10 min at room temperature, radiochemical purity was determined using No. 1 paper chromatography strips (Whatman Ltd., Maidstone, England) prespotted with ethanol and developed in diethyl ether.

Received Jul. 20, 1998; revision accepted Jul. 14, 1999.

For correspondence and reprints contact: A. Michael Rauth, PhD, Experimental Therapeutics, Ontario Cancer Institute, 610 University Ave., Toronto, M5G 1X5, Canada.

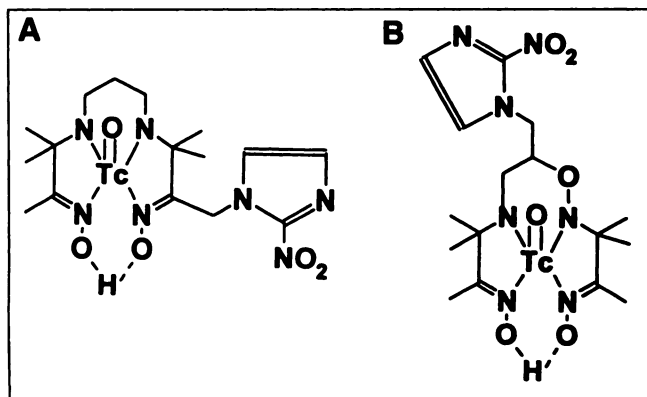


**FIGURE 1.** Chemical structures of (A) BMS181321 and (B) BRU59-21.

BRU59-21 migrated to the top half of the strip, whereas the hydrophilic or insoluble impurities remained near the origin; specifically, the expected impurities ( $^{99m}\text{Tc}$ -pertechnetate,  $^{99m}\text{Tc}$ -DTPA, and  $^{99m}\text{Tc}$  colloid) all had  $R_f$  values  $< 0.3$ . Initial radiochemical purity was  $>90\%$ , and this determination was repeated over time to follow the stability of the complex. The radiopharmaceutical was further diluted with saline to a concentration of 5–10 MBq/mL for in vitro and animal experiments. For determination of partition coefficient, BRU59-21 was first purified using a solid-phase extraction cartridge, then partitioned between equal volumes of presaturated 1-octanol and phosphate-buffered saline (PBS). Purification was accomplished by passing the reaction mixture through a  $\text{C}_{18}$  Sep-Pak Classic (Waters Corp., Milford, MA), which had been activated with methanol and distilled water, washing off hydrophilic impurities with 5 mL water, then eluting BRU59-21 with 0.5-mL aliquots of absolute ethanol. Preparation and evaluation of BMS181321,  $^{99m}\text{Tc}$ -PnAO, and  $^{99m}\text{Tc}$ -5-oxa-PnAO (BMS187047) were performed in an analogous manner as described previously (8).

#### Accumulation of BRU59-21 in Cells

Chinese hamster ovary (CHO) cells, subclone AA8-4, were grown in suspension culture at  $37^\circ\text{C}$  in  $\alpha$ -minimum essential medium plus 10% fetal calf serum (Sigma Chemical Co., St. Louis, MO) (growth medium) as described previously (8,15). For accumulation experiments, 10-mL aliquots of the cell suspension ( $1 \times 10^6$  cells/mL in fresh growth medium) were placed in glass vials and equilibrated for 30 min, with stirring at  $37^\circ\text{C}$  under a continual flow of a prehumidified gas mixture of nitrogen containing 5%  $\text{CO}_2$  and  $<10$  ppm oxygen (hypoxic exposure) or air containing 5%  $\text{CO}_2$  (aerobic exposure) (8). After equilibration, 300  $\mu\text{L}$  diluted BRU59-21 or BMS181321 ( $\sim 2$  MBq) were added, and after 5, 60, 120, 180, and 240 min, samples of  $\sim 400$   $\mu\text{L}$  were removed from the vials without disturbing the oxygenation status of cells in the vial. From these samples, duplicate aliquots of 100  $\mu\text{L}$  were centrifuged through a 1-mL oil gradient (dibutyl phthalate:corn oil, 4:1) in a refrigerated microcentrifuge. The aqueous medium and most of the oil phase were carefully aspirated, and the tip of the tube containing the cell pellet was clipped off and assayed in a  $\gamma$  well counter. The counts in the pellet were expressed as a ratio of radioactivity concentration in the cell to that in the supernatant ( $C_{in}/C_{out}$ ), as described previously (8,15,16). The oxygen dependency of accumulation was determined using intermediate oxygen concentrations in the gas flowed over the cell suspensions (8). As

an alternative to CHO cells, accumulation was also studied in the human leukemia cell line CCRT-CEM. The chelator portion of the molecule,  $^{99m}\text{Tc}$ -5-oxa-PnAO, was evaluated as a non-nitro-containing control. The competition between BRU59-21 and unlabeled nitroaromatic compounds of varying electron affinity was investigated by adding the unlabeled compound to the cell suspension at 0.1- to 10-mmol concentrations before the addition of BRU59-21 (17).

The chemical form of the radioactivity in the supernatant medium was investigated in 2 ways. Aliquots of 100  $\mu\text{L}$  supernatant medium at each sampling time point were partitioned between ethyl acetate and PBS to monitor the appearance of hydrophilic products of metabolism or decomposition (8). For a limited number of samples, 1.2-mL aliquots of supernatant were passed through a centrifugal filter (Ultrafree-MC; Millipore, Bedford, MA) with a nominal molecular weight cutoff of 10,000. This filtration system removed from the samples serum protein, which could damage the high-performance liquid chromatography (HPLC) column. The recovery of radioactivity in the filtrate was  $>90\%$ . Filtered supernatant medium was analyzed with an HPLC that consisted of a pump (System Gold model 125; Beckman Instruments Inc., Fullerton, CA), ultraviolet absorbance detector at 254 nm (model 166; Beckman), and radioisotope detector set for  $^{99m}\text{Tc}$  (model 171; Beckman). The column was reversed-phase  $\text{C}_{18}$  (Ultrasphere ODS,  $4.6 \times 250$  mm; Beckman) and the solvent system was a 60:40 (percent volume in volume) mixture of acetonitrile and ammonium acetate buffer (0.1 mol, pH 4.6) at a flow rate of 1 mL/min.

#### Imaging and Biodistribution Studies

The biodistribution of BRU59-21 was evaluated in syngenic C3H/HeJ mice bearing the KHT-C murine fibrosarcoma in the left hind leg, as described previously (8). Limited studies were performed with a variety of human tumor cell lines (MCF-7 and T47D breast, LNCaP prostate; American Type Culture Collection, Rockville, MD) growing as xenografts in severe combined immunodeficient mice. The tracer (2 MBq in 0.2 mL) was administered by tail-vein injection, and mice were killed by cervical dislocation at times between 10 min and 24 h after injection. Tissue samples were excised and weighed, and their radioactivity was measured in a  $\gamma$  well counter along with an appropriate dilution of the dose. One group of animals received an intravenous injection of nitro-L-arginine (10 mg/kg) 5 min after the tracer; this dose has been shown to increase the hypoxic fraction in KHT-C tumors (18).

## RESULTS

#### Chemical Properties of BRU59-21

BRU59-21 was prepared by addition of  $^{99m}\text{Tc}$ -pertechnetate to kits. The initial labeling efficiency of BRU59-21 was  $93.5\% \pm 1.5\%$  (mean  $\pm$  SD;  $n = 9$ ), slightly higher than for BMS181321 ( $92.1\% \pm 1.4\%$ ;  $n = 18$ ). BRU59-21 was much more stable in vitro, showing a decomposition half-life of  $120 \pm 35$  h ( $n = 6$ ),  $\sim 5$  times longer than that of BMS181321 at the same radioactivity concentration of 185 MBq/mL in saline at room temperature ( $26 \pm 11$  h;  $n = 8$ ). The major decomposition product of both BRU59-21 and BMS181321 appears to be  $^{99m}\text{Tc}$ -pertechnetate. The octanol-water partition coefficient of BRU59-21 was  $11.0 \pm 0.8$  ( $n = 4$ ), substantially lower than that of BMS181321 ( $40.3 \pm 2.2$ ,  $n = 6$ ). The values obtained for BMS181321 were consistent with previously reported data (8).

### Accumulation of BRU59-21 in CHO Cells

The general pattern observed with BRU59-21 was similar to that of BMS181321 as shown in Figures 2B and A, respectively. Under aerobic conditions, BRU59-21 rapidly accumulated in CHO cells to a  $C_{in}/C_{out}$  value of  $\sim 10$ , with little further accumulation over 4 h (Fig. 2B). In contrast, in hypoxic cells this initial accumulation was followed by continuous and extensive accumulation, so that after 4 h there was a 5-fold differential between hypoxic and aerobic accumulation of tracer. This accumulation was accompanied by a change in the chemical form of the radioactivity in the supernatant as shown in Figure 2D. Under aerobic conditions, initially  $\sim 90\%$  of the radioactivity was extractable into ethyl acetate, which reflects the radiochemical purity of the tracer, and only a slight decrease in extractability was seen over 4 h (Fig. 2D). In the supernatant of hypoxic cells, however, there was a continuous decrease in the extractability of radioactivity with time, indicating the production of hydrophilic metabolites. However, this difference did not reach statistical significance, because of large SDs. Similar

results were obtained with the human leukemia cell line CEM (data not shown). The results obtained with BMS181321 in this study were similar to those reported previously (8).

Although this pattern was qualitatively similar to that observed with BMS181321 (Figs. 2A and C), there were quantitative differences. Cellular accumulation of BRU59-21 under both aerobic and hypoxic conditions was lower than that of BMS181321 (note the difference in scale in Figs. 2A and B), reflecting the difference in partition coefficient, but the hypoxic-aerobic differential was actually higher for BRU59-21 ( $5.1 \pm 1.3$ ,  $n = 5$ ; compared with  $3.6 \pm 1.1$ ,  $n = 5$ , for BMS181321). In contrast to the cellular accumulation results, the rate and extent of appearance of hydrophilic metabolites in the supernatant were similar for BMS181321 and BRU59-21 (Figs. 2C and D, respectively).

The disappearance of parent drug and appearance of radiolabeled metabolites in the supernatants of cell suspensions were studied further using radio-HPLC analysis. Representative radiochromatograms are presented in Figure

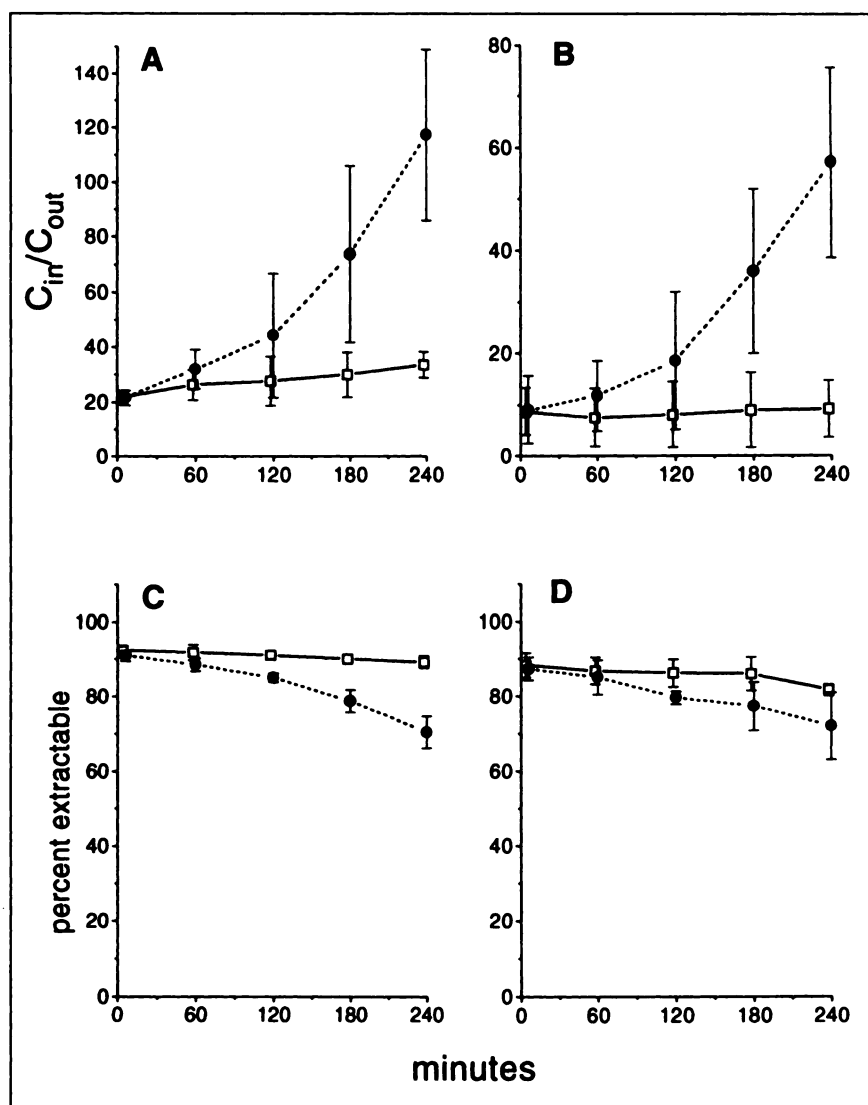


**FIGURE 2.** In vitro experiments with BMS181321 and BRU59-21 in suspensions of CHO cells under aerobic or hypoxic conditions as function of time. Each point is mean  $\pm$  SD for 5 experiments.  $\square$  = aerobic incubation;  $\bullet$  = hypoxic incubation. Accumulation of radioactivity in cells is expressed as ratio of activity concentration in cells to that in supernatant,  $C_{in}/C_{out}$  for (A) BMS181321 and (B) BRU59-21. Note difference in scale. Effect of incubation conditions and time on extractability into ethyl acetate of radioactivity in supernatant is shown for (C) BMS181321 and (D) BRU59-21.

3 and quantitative analysis in Table 1. Figure 3A presents the tracing for analysis of a sample of supernatant taken 5 min after addition of BRU59-21 to a cell suspension at  $10^6$  cells/mL incubated under hypoxic conditions. Intact BRU59-21 had a retention time of 8.2 min and represented 89.4% of the total peak area. An impurity peak at 4.1 min comprised 4.7% of the total peak area. The pattern was the same in samples removed at 5 min from suspensions incubated under aerobic conditions as shown in Table 1. After 4 h there was little change in the chromatographic tracings for the aerobic incubations, with  $>80\%$  of the radioactivity remaining as the parent compound (Table 1). In contrast, incubation for 4 h under hypoxic conditions resulted in a substantial loss of the parent compound, so that it constituted only 30% of the total peak area. At the same time there was extensive production (60% peak area) of a metabolite or metabolites with the same retention time as the initial impurity (Fig. 3B; Table 1). This is also the same retention time as for  $^{99m}\text{Tc}$ -pertechnetate. In all samples

**TABLE 1**  
Radio-HPLC Analysis of Supernatant Medium  
from Cell Suspensions

Incubation time (min)	Retention time (min)	Aerobic		Hypoxic	
		Peak area %	Range	Peak area %	Range
5	4.1	6.6	4.4–8.7	5.9	4.7–7.1
	8.2	86.3	86.1–86.7	88.0	86.7–89.4
240	4.1	11.2	10.2–12.4	60.0	58.3–61.4
	8.2	83.0	81.8–83.7	30.1	28.1–33.8

analyzed, the areas under these 2 peaks constituted  $>90\%$  of the total peak area. Thus, the presence of hypoxic cells led to increased production of metabolites.

The accumulation of BRU59-21 in hypoxic cells was subject to competition from oxygen and other electron-affinic compounds. From experiments performed with different concentrations of oxygen flowing over the cell suspension and correction for respiration of oxygen by the cells as described previously (8), it was determined that the oxygen level that results in 50% inhibition of accumulation was 40 ppm (data not shown), which is similar to that reported for BMS181321 in the same system (8). Addition of 8 mmol misonidazole, a 2-nitroimidazole with an electron affinity expected to be similar to that of BRU59-21, dramatically reduced the hypoxia-selective accumulation of radioactivity to  $6.0\% \pm 5.1\%$  ( $n = 3$ ) of control values at 4 h. In contrast, in the presence of 9 mmol tinidazole, a 5-nitroimidazole with lower electron affinity, accumulation of radioactivity in hypoxic cells was enhanced to  $230\% \pm 70\%$  ( $n = 3$ ) of control values. The effects of misonidazole or tinidazole on accumulation of BRU59-21 were less extensive at lower concentrations of the competing agent and were also reflected in the extent of metabolism evident in the supernatant (data not shown). Neither misonidazole nor tinidazole affected accumulation under aerobic conditions (data not shown). These effects of competing nitro compounds on tracer accumulation under hypoxia are similar to those reported for BMS181321 (17).

As a negative control, experiments were performed with the chelator portion of the molecule,  $^{99m}\text{Tc}$ -5-oxa-PnAO. Although the initial accumulation of  $^{99m}\text{Tc}$ -5-oxa-PnAO was similar to that of BRU59-21, reflecting its similar partition coefficient, no hypoxic-aerobic differential developed with time as occurs with the 2-nitroimidazole-containing molecules (data not shown).

#### Tumor Imaging in Mice

After intravenous injection, BRU59-21 showed rapid clearance from the blood, penetration of all tissues, and prompt excretion through the liver into the intestinal tract, with  $\sim 70\%$  of the dose being eliminated by this route (Table 2). In contrast, urinary elimination was minimal ( $<10\%$ ). The tracer was delivered to the tumor efficiently but showed significant washout over time. However, clearance from background tissues such as blood and muscle was more rapid, so that tumor-to-blood and tumor-to-muscle ratios

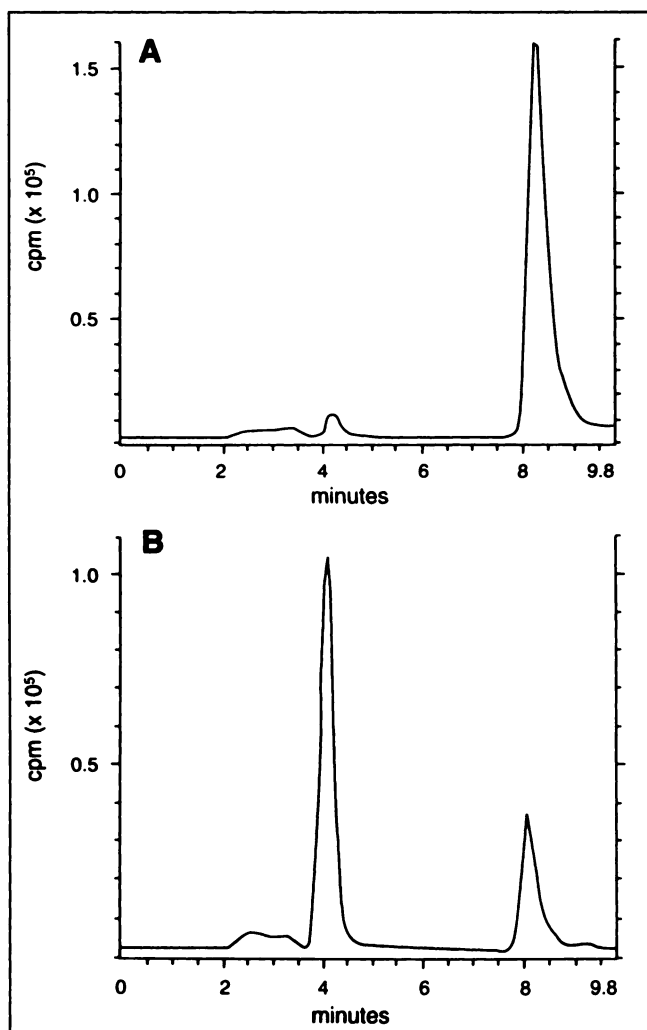


**FIGURE 3.** HPLC radiochromatograms of samples from supernatant medium after 5 (A) and 240 (B) min incubation of BRU59-21 with CHO cells under hypoxic conditions. Retention time of intact BRU59-21 was 8.2 min.

TABLE 2

Time Course of Biodistribution of Radioactivity After Intravenous Administration of BRU59-21 to Mice Bearing KHT-C Tumors

Tissue	10 min	1 h	2 h	4 h	6 h	8 h	24 h
<b>%ID/g tissue</b>							
Blood	1.56 ± 0.43	0.53 ± 0.05	0.43 ± 0.07	0.40 ± 0.08	0.36 ± 0.10	0.32 ± 0.10	0.20 ± 0.05
Heart	0.90 ± 0.26	0.43 ± 0.15	0.31 ± 0.04	0.22 ± 0.08	0.25 ± 0.05	0.21 ± 0.04	0.16 ± 0.04
Lung	1.22 ± 0.26	0.67 ± 0.12	0.52 ± 0.07	0.47 ± 0.17	0.49 ± 0.12	0.36 ± 0.06	0.25 ± 0.05
Liver	14.32 ± 2.52	8.63 ± 1.73	8.37 ± 0.87	6.77 ± 2.21	4.78 ± 1.62	2.65 ± 0.63	1.77 ± 0.58
Spleen	1.19 ± 0.31	0.62 ± 0.08	0.60 ± 0.10	0.51 ± 0.15	0.44 ± 0.10	0.34 ± 0.10	0.25 ± 0.09
Kidney	4.65 ± 0.95	2.17 ± 0.29	1.89 ± 0.55	1.70 ± 1.12	1.55 ± 0.47	0.75 ± 0.06	0.56 ± 0.10
Skeletal muscle	0.43 ± 0.16	0.11 ± 0.01	0.09 ± 0.01	0.08 ± 0.02	0.08 ± 0.02	0.06 ± 0.02	0.06 ± 0.01
Tumor	0.73 ± 0.22	0.37 ± 0.04	0.37 ± 0.14	0.31 ± 0.18	0.29 ± 0.11	0.17 ± 0.02	0.16 ± 0.07
<b>%ID/region</b>							
Intestinal contents	54.6 ± 8.4	67.8 ± 5.3	71.8 ± 1.6	55.5 ± 18.6	27.0 ± 6.9	7.2 ± 3.0	5.9 ± 0.5
Urinary bladder	3.7 ± 1.5	4.8 ± 2.3	5.4 ± 3.3	NM	NM	NM	NM
Whole body	100	94.0 ± 5.9	93.8 ± 6.0	78.1 ± 11.5	43.0 ± 2.8	16.2 ± 3.7	17.4 ± 10.4
<b>Ratios</b>							
Tumor to muscle	1.62 ± 0.29	3.56 ± 0.33	3.84 ± 1.54	4.37 ± 1.69	3.55 ± 0.90	3.27 ± 0.86	2.65 ± 0.87
Tumor to blood	0.47 ± 0.04	0.71 ± 0.12	0.86 ± 0.21	0.95 ± 0.44	0.94 ± 0.27	0.62 ± 0.20	0.80 ± 0.36

Each value is mean ± SD for 4–6 mice.  
NM = not measurable.

increased to their maximums at 4 h after injection (Table 2; Figs. 4C and B, respectively).

Levels of BRU59-21 in all tissues were lower than those of BMS181321 (8) and this difference began very early, with only the liver having comparable levels at 10 min. Results for absolute levels in tumor and tumor-to-background ratios are compared in Figure 4 for the present BRU59-21 data and the previously reported BMS181321 data (8). Most important, clearance from blood and muscle was particularly rapid with BRU59-21, contributing to improved imaging characteristics. However, excretion of BRU59-21 into the intestine

was at least as extensive as of BMS181321, for which complete data are not available (8). This results in high background radioactivity in the abdomen, which can interfere with tumor imaging. In a limited number of experiments in SCID mice bearing a variety of human tumors (MCF-7 and T47D breast, LNCaP prostate), biodistribution and tumor localization of BRU59-21 were similar to what was observed in murine tumors (data not shown).

Injection of nitro-L-arginine, an inhibitor of nitric oxide synthase which has been shown to increase the hypoxic fraction in KHT-C tumors (18), resulted in higher levels of

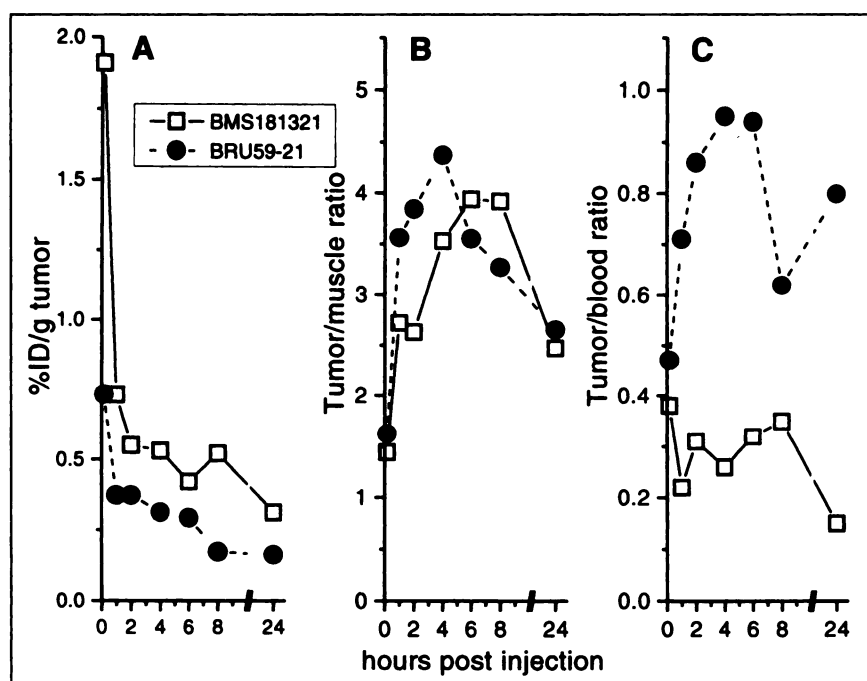


**FIGURE 4.** Comparison of time course of biodistribution of BMS181321 (□) and BRU59-21 (●) in mice bearing transplanted KHT-C tumor. (A) %ID/g tumor, (B) tumor-to-muscle ratio, and (C) tumor-to-blood ratio. Each point is mean value for 4–13 mice.

radioactivity in the tumor when animals were killed 4 h later (Table 3). There were no significant effects on radioactivity levels in blood, muscle, or other tissues (data not shown). This response to nitro-L-arginine is similar to that reported for BMS181321 (8).

## DISCUSSION

It is the goal of hypoxia imaging to assess the fraction of hypoxic cells in individual tumors. Tumors that are identical by all standard clinical criteria can differ widely in their degree of hypoxia, and extensive tumor hypoxia is a prognostic factor for poor survival after both radiotherapeutic and surgical treatment in certain types of cancer. The ideal hypoxia imaging agent should meet the following criteria. It should be (a) easily prepared, (b) easily administered systemically, (c) rapidly accumulated and specifically retained in hypoxic tumor cells, (d) rapidly cleared from background tissues, and (e) noninvasively detected at high resolution with equipment generally available in most hospitals. The present results suggest that BRU59-21 fully meets criteria a and b. Its specificity for hypoxic tumor cells (criteria c and d), though comparable to that of other radiolabeled hypoxic cell markers, is not optimal but may be adequate. Its tumor localization can be detected noninvasively by standard planar and SPECT nuclear medicine cameras but with a resolution limit typical for  $^{99m}\text{Tc}$ -labeled compounds (criterion e). In the following, the results leading to these conclusions are discussed in detail.

Interest in  $^{99m}\text{Tc}$ -labeled nitroimidazole derivatives was sparked by the success in imaging tumor hypoxia using  $^{18}\text{F}$ -fluoromisonidazole with PET (19) and  $^{123}\text{I}$ -iodoazomycin arabinoside with SPECT (20). However, problems of availability or cost of these techniques led to attempts to prepare a  $^{99m}\text{Tc}$  analog. Evaluation of BMS181321, a 2-nitroimidazole coupled to a propylene amine oxime chelator, in models of tumor hypoxia has been reported from this laboratory (8). Although BMS181321 offered proof of the principle that a  $^{99m}\text{Tc}$ -labeled 2-nitroimidazole could be used

to image hypoxia in tumors, the potential utility of this compound was limited by its high lipophilicity, which contributed to slow clearance of background radioactivity and suboptimal tumor-to-muscle and tumor-to-blood ratios. In addition, it was unstable in solution, with a half-life of 16–20 h.

BRU59-21, the second-generation compound studied in the present report, differs in structure from BMS181321 in the replacement of a methylene unit in the propylene bridge by an oxygen molecule and in moving the point of attachment to the 2-nitroimidazole (Fig. 1). These modifications have the result of increasing chemical stability and reducing partition coefficient, both of which are considered advantages. The *in vitro* properties of BRU59-21 are essentially identical to those of BMS181321 (Figs. 2A and B). BRU59-21 showed selective accumulation in hypoxic cells, although the slopes of the accumulation curves for BMS181321 were quantitatively different from those reported previously (8), showing an initial lag in accumulation before linear uptake occurred. This difference was ultimately traced to batch-to-batch variations in the corn oil used in the cell separation step. Despite this difference from previous results, the present data convincingly show the similar behaviors of BMS181321 and BRU59-21.

The selective appearance of metabolites in the supernatant of hypoxic cell suspensions was seen for BMS181321 and BRU59-21 as decreases in the percent of the radioactivity extractable into ethyl acetate (Figs. 2C and D). In addition, HPLC data for BRU59-21 (Fig. 3) indicate that this decrease can be accounted for by the production of a metabolite or metabolites moving as a single, more hydrophilic peak. Testing in a second HPLC solvent system (methanol:water) again showed a single metabolite peak (data not shown), but confirmation of a single metabolite or multiple metabolites will require further study.

The oxygen dependency of this accumulation is extremely low, and accumulation can be modulated in a dose-dependent manner by the presence of nitro compounds of different electron affinities. Absolute uptake of BRU59-21 is lower than of BMS181321, in keeping with its lower partition coefficient; however, the resultant hypoxic-aerobic differential is similar (Fig. 2).

Hypoxic coincubation results for BRU59-21 with the 2-nitroimidazole misonidazole (inhibition of accumulation) and the 5-nitroimidazole tinidazole (stimulation of accumulation) parallel earlier results with BMS181321 (17). To what degree these effects are the result of a competition for cellular reducing equivalents or transfer of electrons from 1 radical anion species to another has yet to be determined. Clearly, large excess concentrations of the unlabeled nitroimidazoles are required to show this effect.

It was important to run as a control the chelator portion of the molecule alone, in light of the recent unanticipated hypoxia-specific accumulation of  $^{99m}\text{Tc}$ -labeled butylene amine oxime or  $^{99m}\text{Tc}$ -HL91 (21–23), a homolog of  $^{99m}\text{Tc}$ -PnAO. Both  $^{99m}\text{Tc}$ -PnAO and  $^{99m}\text{Tc}$ -5-oxa-PnAO partition

**TABLE 3**  
Effect of Modulation of Tumor Hypoxia by Injection of Nitro-L-Arginine 5 Minutes After BRU59-21 in Mice Bearing KHT-C Tumors

Tissue	Controls (n = 5)	Nitro-L-Arginine (n = 4)	P
%ID/g			
Blood	0.353 ± 0.076	0.337 ± 0.033	NS
Muscle	0.069 ± 0.010	0.068 ± 0.006	NS
Tumor	0.263 ± 0.017	0.397 ± 0.068	<0.005
Ratios			
Tumor to muscle	3.84 ± 0.49	5.67 ± 1.15	<0.025
Tumor to blood	0.77 ± 0.15	1.17 ± 0.19	<0.01
Tumor weight (g)	1.35 ± 0.23	1.28 ± 0.17	NS

Each value is mean ± SD for mice killed 4 h after injection.  
NS = not significant.

into cells but do not show selective accumulation in hypoxic cells.

When administered to mice bearing KHT-C tumors, BRU59-21 was efficiently distributed to the tissues; however, levels in all tissues were lower than those observed with BMS181321 in the same model system (8), again presumably reflecting the role of partition coefficient. Although maximum tumor-to-muscle ratios were similar for the 2 analogs, BRU59-21 offered superior tumor-to-blood ratios because of more extensive clearance from blood (Fig. 4). However, this improved clearance appeared to be the result of more rapid excretion through the liver into the intestinal tract and not of a shift from hepatic to renal elimination. Therefore, BRU59-21 shares the problem of BMS181321 of high background radioactivity in the abdomen. Thus, tumor imaging with BRU59-21 would not necessarily be improved to the same extent that cardiac imaging is improved (14). However, BRU59-21 does offer promise for imaging hypoxia in tumors outside the abdomen, such as those of the head and neck and of the breast, in which hypoxia is believed to be an impediment to local control by radiotherapy (23–26). The experiments in which nitro-L-arginine was used to increase hypoxic cell fraction and BRU59-21 accumulation specifically in tumors (Table 3) show the utility of BRU59-21 in measuring transient changes in tumor oxygenation. Increasing the oxygen concentration in gases breathed by patients undergoing radiotherapy to decrease hypoxic cell fraction has been extensively studied clinically (27). Thus, BRU59-21 may be useful for monitoring directly the effects of such procedures in individual patients.

When these results are compared with those of other tracers evaluated in similar murine tumor model systems (8,28,29), the tumor-to-muscle ratios at 2 h after injection obtained with BRU59-21 are as high as with any of the reported compounds (Table 4). Furthermore, BRU59-21 may be useful also for imaging of hypoxia in other conditions, such as anaerobic infections, rheumatoid arthritis, and peripheral vascular disease, in which <sup>18</sup>F-FMISO and <sup>123</sup>I-IAZA show promise (30,31).

**TABLE 4**  
Comparison of Tumor-to-Background Ratios in Murine Tumor Models at 2 Hours After Injection of Some Radiolabeled 2-Nitroimidazoles

Compound	Tumor to blood	Tumor to muscle	n	Reference
<sup>3</sup> H-misonidazole	1.88 ± 0.62	1.54 ± 0.57	5*	(28)
<sup>3</sup> H-FMISO	1.32 ± 0.20	1.42 ± 0.16	5†	(28)
<sup>125</sup> I-IAZA	2.80 ± 1.71	3.70 ± 2.26	6†	(29)
<sup>99m</sup> Tc-BMS181321	0.31 ± 0.05	2.63 ± 0.57	9*	(8)
<sup>99m</sup> Tc-BRU59-21	0.86 ± 0.21	3.84 ± 1.54	6*	(this article)

\*KHT tumor in C3H mice.

†EMT-6 tumor in BALB/c mice.

Each value is mean ± SD for n mice.

## CONCLUSION

BRU59-21 has been shown to be significantly more stable in saline and growth medium than the first-generation compound BMS181321, as well as more hydrophilic. BRU59-21 has been evaluated in models of tumor hypoxia in vitro and in mice. Its properties in vitro are similar to those of BMS181321. In mice, BRU59-21 shows more rapid clearance from blood and enhanced tumor-to-blood ratios. These properties make BRU59-21 attractive for further investigation as an agent for imaging tumor hypoxia in the clinic.

## ACKNOWLEDGMENTS

The authors thank Bob Kuba for assistance with the animal studies. This work was supported by operating grants from the Medical Research Council of Canada and the National Cancer Institute of Canada and by personal financial support from a University of Toronto Open Fellowship and a Pharmaceutical Manufacturers Association of Canada Scholarship. The authors thank Drs. Adrian Nunn and Karen Linder of Bracco Research USA for supplying kits for the preparation of BMS181321 and BRU59-21. CCRT-CEM was obtained from Dr. William T. Beck, St. Jude's Hospital, Memphis, TN, through Dr. Ian F. Tannock, Ontario Cancer Institute, Toronto, Canada.

## REFERENCES

- Linder KE, Chan Y-W, Cyr JE, Malley MF, Nowotnik DP, Nunn AD. TcO(PnAO-1-(2-nitroimidazole)) [BMS-181321], a new technetium-containing nitroimidazole complex for imaging hypoxia: synthesis, characterization, and xanthine oxidase-catalyzed reduction. *J Med Chem.* 1994;37:9–17.
- Nunn A, Linder K, Strauss HW. Nitroimidazoles and imaging hypoxia. *Eur J Nucl Med.* 1995;22:265–280.
- DiRocco RJ, Kuczynski BL, Pirro JP, et al. Imaging ischemic tissue at risk of infarction during stroke. *J Cereb Blood Flow Metab.* 1993;13:755–762.
- Rumsey WL, Cyr JE, Raju N, Narra RK. A novel [<sup>99m</sup>Tc]technetium-labeled nitroheterocycle capable of identification of hypoxia in heart. *Biochem Biophys Res Commun.* 1993;193:1239–1246.
- Kusuoka H, Hashimoto K, Fukuchi K, Nishimura T. Kinetics of a putative hypoxic tissue marker, technetium-99m-nitroimidazole (BMS181321), in normoxic, hypoxic, ischemic and stunned myocardium. *J Nucl Med.* 1994;35:1371–1376.
- Rumsey WL, Kuczynski B, Patel B, et al. SPECT imaging of ischemic myocardium using a technetium-99m-nitroimidazole ligand. *J Nucl Med.* 1995;36:1445–1450.
- Ng CK, Sinusas AJ, Zaret BL, Stouffer R. Kinetic analysis of technetium-99m-labeled nitroimidazole (BMS-181321) as a tracer of myocardial hypoxia. *Circulation.* 1995;92:1261–1268.
- Ballinger JR, Wan Min Kee J, Rauth AM. In vitro and in vivo evaluation of a technetium-99m-labeled 2-nitroimidazole (BMS181321) as a marker of tumor hypoxia. *J Nucl Med.* 1996;37:1023–1031.
- Okada RD, Nguyen KN, Strauss HW, Johnson G. Effects of low flow and hypoxia on myocardial retention of technetium-99m BMS181321. *Eur J Nucl Med.* 1996;23:443–447.
- Fukuchi K, Kusuoka H, Watanabe Y, Fujiwara T, Nishimura T. Ischemic and reperfused myocardium detected with technetium-99m-nitroimidazole. *J Nucl Med.* 1996;37:761–766.
- DiRocco RJ, Bauer AA, Pirro JP, et al. Delineation of the border zone of ischemic rabbit myocardium by a technetium-labeled nitroimidazole. *Nucl Med Biol.* 1997;24:201–207.
- Barron B, Grotta J, Lamki L, et al. Preliminary experience with technetium-99m BMS-181321, a nitroimidazole, in the detection of cerebral ischemia associated with acute stroke [abstract]. *J Nucl Med.* 1996;37(suppl):272P–273P.

13. Wedeking P, Yost F, Wen M, et al. Comparison of the biologic activity of the isomers of the Tc-99m-nitroimidazole complex BMS-194796 [abstract]. *J Nucl Med.* 1995;36(suppl):17P.
14. Johnson LL, Schofield L, Mastrofrancesco P, Donahay T, Nott L. Technetium-99m-nitroimidazole uptake in a swine model of demand ischemia. *J Nucl Med.* 1998;39:1468-1475.
15. Ballinger JR, Cowan DSM, Boxen I, Zhang ZM, Rauth AM. Effect of hypoxia on the accumulation of technetium-99m-glucurate and technetium-99m-gluconate by Chinese hamster ovary cells in vitro. *J Nucl Med.* 1993;34:242-245.
16. Cowan DSM, Melo T, Park L, Ballinger JR, Rauth AM. BMS181321 accumulation in rodent and human cells: the role of P-glycoprotein. *Br J Cancer.* 1996;74(suppl):S264-S266.
17. Melo T, Hua HA, Ballinger JR, Rauth AM. Modifying the in vitro accumulation of BMS181321, a technetium-99m-nitroimidazole, with unlabelled nitroaromatics. *Biochem Pharmacol.* 1997;54:685-693.
18. Wood PJ, Stratford U, Adams GE, Szabo C, Thiemermann C, Vane JR. Modification of energy metabolism and radiation response of a murine tumor by changes to nitric oxide availability. *Biochem Biophys Res Commun.* 1993;192:505-510.
19. Koh W-J, Rasey JS, Evans ML, et al. Imaging of hypoxia in human tumors with [<sup>18</sup>F]-fluoromisonidazole. *Int J Radiat Oncol Biol Phys.* 1991;22:199-212.
20. Parliament MB, Chapman JD, Urtasun RC, et al. Noninvasive assessment of human tumor hypoxia with <sup>125</sup>I-iodoazomycin arabinoside: preliminary report of a clinical study. *Br J Cancer.* 1992;65:90-95.
21. Archer CM, Edwards B, Kelly JD, King AC, Burke JF, Riley ALM. Technetium-labelled agents for imaging tissue hypoxia in vivo. In: Nicolini M, Bandoli G, Mazzi U, eds. *Technetium and Rhenium in Chemistry and Nuclear Medicine.* Padova, Italy: SG Editoriali; 1995:535-539.
22. Okada RD, Johnson G, Nguyen KN, Edwards B, Archer CM, Kelly JD. <sup>99m</sup>Tc-HL91: effects of low flow and hypoxia on a new ischemia-avid myocardial imaging agent. *Circulation.* 1997;95:1892-1899.
23. Cook GJR, Houston S, Barrington SF, Fogelman I. Technetium-99m-labeled HL91 to identify tumor hypoxia: correlation with fluorine-18-FDG. *J Nucl Med.* 1998;39:99-103.
24. McEwan AJB, Catz Z, Morin C, Wiebe LI. Hypoxia imaging in patients with breast cancer [abstract]. *Eur J Nucl Med.* 1997;24:1028.
25. Nordmark M, Overgaard M, Overgaard J. Pretreatment oxygenation predicts radiation response in advance squamous cell carcinoma of the head and neck. *Radiother Oncol.* 1996;41:31-39.
26. Brizel DM, Sibley GS, Prosnitz LR, Scher RL, Dewhirst MW. Tumor hypoxia adversely affects the prognosis of carcinoma of the head and neck. *Int J Radiat Oncol Biol Phys.* 1997;38:285-289.
27. Overgaard J, Horsman MR. Modification of hypoxia-induced radioresistance in tumors by the use of oxygen and sensitizers. *Semin Radiat Oncol.* 1996;6:10-21.
28. Grunbaum Z, Freauff SJ, Krohn KA, Wilbur DS, Magee S, Rasey JS. Synthesis and characterization of congeners of misonidazole for imaging hypoxia. *J Nucl Med.* 1987;28:68-75.
29. Mannan RH, Somayaji VV, Lee J, Mercer JR, Chapman JD, Wiebe LI. Radioiodinated 1-(5-iodo-5-deoxy-beta-D-arabinofuranosyl)-2-nitroimidazole (iodoazomycin arabinoside: IAZA): a novel marker of tissue hypoxia. *J Nucl Med.* 1991;32:1764-1770.
30. McEwan AJB, Skeith KJ, Mannan RH, et al. I-123 iodoazomycin arabinoside (IAZA) may have a role in imaging rheumatoid arthritis [abstract]. *J Nucl Med.* 1997;38(suppl):300P-301P.
31. Liu R-S, Chu L-C, Yen S-H, et al. Detection of anaerobic odontogenic infections by fluorine-18 fluoromisonidazole. *Eur J Nucl Med.* 1996;23:1384-1387.